

NASA/TM-2013-218050



Material Property Characterization of AS4/VRM-34 Textile Laminates

Ray W. Grenoble
Langley Research Center, Hampton, Virginia

William M. Johnston
Science and Technology Corporation, Hampton, Virginia

October 2013

NASA STI Program . . . in Profile

Since its founding, NASA has been dedicated to the advancement of aeronautics and space science. The NASA scientific and technical information (STI) program plays a key part in helping NASA maintain this important role.

The NASA STI program operates under the auspices of the Agency Chief Information Officer. It collects, organizes, provides for archiving, and disseminates NASA's STI. The NASA STI program provides access to the NASA Aeronautics and Space Database and its public interface, the NASA Technical Report Server, thus providing one of the largest collections of aeronautical and space science STI in the world. Results are published in both non-NASA channels and by NASA in the NASA STI Report Series, which includes the following report types:

- **TECHNICAL PUBLICATION.** Reports of completed research or a major significant phase of research that present the results of NASA Programs and include extensive data or theoretical analysis. Includes compilations of significant scientific and technical data and information deemed to be of continuing reference value. NASA counterpart of peer-reviewed formal professional papers, but having less stringent limitations on manuscript length and extent of graphic presentations.
- **TECHNICAL MEMORANDUM.** Scientific and technical findings that are preliminary or of specialized interest, e.g., quick release reports, working papers, and bibliographies that contain minimal annotation. Does not contain extensive analysis.
- **CONTRACTOR REPORT.** Scientific and technical findings by NASA-sponsored contractors and grantees.

- **CONFERENCE PUBLICATION.** Collected papers from scientific and technical conferences, symposia, seminars, or other meetings sponsored or co-sponsored by NASA.
- **SPECIAL PUBLICATION.** Scientific, technical, or historical information from NASA programs, projects, and missions, often concerned with subjects having substantial public interest.
- **TECHNICAL TRANSLATION.** English-language translations of foreign scientific and technical material pertinent to NASA's mission.

Specialized services also include organizing and publishing research results, distributing specialized research announcements and feeds, providing information desk and personal search support, and enabling data exchange services.

For more information about the NASA STI program, see the following:

- Access the NASA STI program home page at <http://www.sti.nasa.gov>
- E-mail your question to help@sti.nasa.gov
- Fax your question to the NASA STI Information Desk at 443-757-5803
- Phone the NASA STI Information Desk at 443-757-5802
- Write to:
STI Information Desk
NASA Center for AeroSpace Information
7115 Standard Drive
Hanover, MD 21076-1320

NASA/TM-2013-218050



Material Property Characterization of AS4/VRM-34 Textile Laminates

*Ray W. Grenoble
Langley Research Center, Hampton, Virginia*

*William M. Johnston
Science and Technology Corporation, Hampton, Virginia*

National Aeronautics and
Space Administration

Langley Research Center
Hampton, Virginia 23681-2199

October 2013

The use of trademarks or names of manufacturers in this report is for accurate reporting and does not constitute an official endorsement, either expressed or implied, of such products or manufacturers by the National Aeronautics and Space Administration.

Available from:

NASA Center for AeroSpace Information
7115 Standard Drive
Hanover, MD 21076-1320
443-757-5802

Abstract

Several material properties (modulus, strengths, and fracture toughness) of a textile composite have been evaluated to provide input data to analytical models of Pultruded Rod Stiffened Efficient Unitized Structure (PRSEUS). The material system is based on warp-knitted preforms of AS4 carbon fibers and VRM-34 epoxy resin, which have been processed via resin infusion and oven curing. Tensile, compressive, shear, and fracture toughness properties have been measured at ambient and elevated temperatures. All specimens were tested in as-fabricated (dry) condition. Specimens were tested with and without through-thickness stitching.

Introduction

Development work on the Pultruded Rod Stiffened Efficient Unitized Structure^{1,2} (PRSEUS) concept has recently progressed via collaborative work between NASA and Boeing on the Hybrid Wing Body aircraft (HWB). The HWB is a design for a future airliner, based on a flying wing configuration. The width of the aircraft's body center section results in a pressurized cabin with a rectangular cross-sectional shape. Whereas a conventional (elliptical cross-section) fuselage carries most internal pressure-driven loads through skin tension, the flat sides of the HWB pressure cabin will carry those loads primarily via bending.

PRSEUS leverages lessons learned in previous NASA-sponsored textile composites development activities such as the Advanced Composites Technology (ACT) program^{3,4}. ACT focused on development of carbon fiber textile-based composites, which incorporated through-thickness stitching to increase damage tolerance. The development of innovative processing methods to reduce fabrication costs was also pursued. The program culminated with the fabrication (using a resin film infusion process) and testing of a representative wing box structural component with embedded impact damage.

The primary features distinguishing PRSEUS are:

- Skins and stiffening members composed of warp-knitted, multidirectional, dry carbon fiber preforms
- Foam-filled frames covered in one of the aforementioned preforms
- Stringers incorporating a pre-cured, unidirectional carbon/epoxy rod in the upper flange
- Through-thickness stitching between the stringer/frame base flanges and the skin
- Out-of-autoclave processing (via a vacuum-assisted resin infusion process) using low-cost foam assembly tooling and oven cure.

The unidirectional rod in the stringer flanges provides the structure with very high bending stiffness in the longitudinal direction. This attribute makes the concept attractive for application to HWB's pressurized cabin. The stitching at the stiffener/skin bondline is intended to suppress delamination of that critical interface well into a post-buckling loading regime⁵.

During the fabrication process, dry stiffener and frame preforms are assembled upside-down in foam/plastic tooling. The tear straps and skins are placed over the stiffening elements and the constituents are then stitched together through the thickness from what will be the tool side (skin side) of the part. The position of the precured rods in the stringers relative to the skin is established by the holes through the foam cores of the frames. Once the stitched assembly is removed from the tooling, it is effectively self-supporting. This attribute greatly reduces the amount of tooling required during the remainder of the manufacturing process. An illustration of a stringer-frame intersection, which shows how the structure is assembled, is provided in Figure 1.

To date, little material property data for PRSEUS structure have been available in the open literature. This deficit has prevented development of accurate finite element models of this structural concept, and has limited the ability of others outside NASA and Boeing to evaluate the suitability of PRSEUS for their own applications. The present study is intended to address this lack of data by developing a set of elastic material properties for use as input to analytical models of PRSEUS acreage (skin and stiffener webs). Coupons are tested to provide data on the tensile, compressive, and shear properties. All coupons were tested in as-fabricated condition. Testing was performed at 72°F and 180°F. In addition, Mode I and Mode II interlaminar fracture toughness testing was performed to provide data for analysis of debonding and delamination.

Materials

This study evaluates the mechanical properties of balanced, symmetric laminates, fabricated from warp-knitted [0/90]_T preforms of AS4 fiber, and infused with VRM-34 epoxy resin (both from Hexcel Corporation). The thickness of the panels fabricated varied with the requirements of each specimen type, as shown in Table 1. Boeing Research and Technology (Huntington Beach, CA) fabricated the panels and shipped them to NASA Langley Research Center.

Some panels incorporated through-thickness stitching to represent the stitched bondline between the skins and stiffeners. Stitches were formed from 1600 denier Vectran thread at 5.08 stitches per inch. In PRSEUS structure, stitches are placed in pairs. The first stitch enters the skin near the center of the stiffener element lower flange half, and is oriented normal to the skin surface. A second, inclined, stitch is placed on the bag side of the part, adjacent to the stiffener web and exits on the tool side under the stiffener web. Figure 2 illustrates the stitch placement on a typical stringer. Placement of stitches within stitched specimens tested in this work followed a similar scheme. The stitches were placed in pairs; one stitch was oriented normal to the skin surface and one was inclined at a 56° angle relative to the tool surface. All stitch lines were oriented along the length of the specimens. Table 1 shows the complete test matrix.

Characterization

Each specimen set contained six replicates. All specimens were tested in servo-hydraulic test stands. Tensile specimens were loaded through hydraulic wedge grips. Compression, shear, and fracture toughness specimens were tested in test fixtures meeting their respective test standard recommendations. All data analysis was performed in the manner recommended by the relevant ASTM test standards.

Table 1. Test matrix

Test Type	ASTM Test Standard	Test Temperatures, °F	Unstitched	Stitched	Specimen Dimensions [†] , in.	Extensometer / Strain Gages
Tension	D3039	72, 180	Y	Y	12 x 1 x 0.063	back-to-back / back-to-back at 90°
Compression	D6418	72, 180	N	Y	6 x 0.5 x 0.157	none / back-to-back axial
Inplane Shear	D7078	72, 180	Y	Y	2.2 x 3 x 0.157	none / back-to-back at ±45°
Mode I Fracture Toughness	D5229	72, 180	Y	N [†]	7 x 1 x 0.314	none
Mode II Fracture Toughness	ENF Draft	72, 180	Y	Y	7 x 1 x 0.314	none

[†] Test found inapplicable due to failure mode exhibited

[‡] All laminates were symmetric and balanced, and were based on 0/90 and 90/0 preforms of 0.0157 in. thickness.

Specimen Preparation

In general, specimens were cut from their precursor panels using a waterjet. Tensile specimens were tabbed with a balanced, symmetric layup of the same AS4/VRM-34 material used for the specimens. Tabs were 3.5 in. long x 0.063 in. thick, and their ends were tapered at a 6° angle toward the gage section. The tab material was secondarily bonded to the precursor panel using Hysol EA9394™ adhesive and was cured at 150°F for one hour. Individual tensile specimens were then cut from the panel with a diamond-grit grinding wheel mounted on a surface grinder. Axial strains were monitored with a pair of extensometers (MTS Type 632), calibrated over a 0.12-in. length. Transverse strains were monitored via back-to-back transverse strain gages in the center of the gage section.

The edges and ends of compression test specimens were ground flat and parallel by trimming their waterjet-cut edges on a surface grinder, using a diamond-grit cutting wheel. Tabs were made from glass/epoxy laminate (G10), 1/4 in. in thickness. They were secondarily bonded to the panel in a manner identical to that of the tensile specimens. Axial strains were monitored during testing with a pair of back-to-back strain gages, 0.25 in. long, centered in the specimens' 0.5-in. long gage length.

The inplane shear specimens were of the V-notch rail shear configuration. These specimens require geometric tolerances in the gage region that could not be maintained by the waterjet cutter. The final geometry of the notch on these specimens was established with a diamond grit endmill in a milling machine. Shear strains within the gage section were monitored with back-to-back strain gages mounted at +/- 45° angles to the applied load. Stitched shear specimens were cut in two configurations to assess the effects of shear loading along the stitch line. The first configuration placed the line of normal-direction stitches through the center of the notch, as seen in Figure 3(a). The second configuration centered the notch between the two stitch lines, which is shown in Figure 3(b).

Mode I fracture toughness specimens were of the double cantilever beam (DCB) geometry. Load introduction was through adhesive-bonded aluminum hinges. Both types of fracture toughness specimen included an initial delamination, 2.5 in. long, created by inclusion of a 0.0005 in.-thick Teflon film in the specimen midplane. Mode II fracture specimens were tested in an end notched flexure (ENF) configuration. They required no preparation beyond waterjet cutting and applying the appropriate markings to the specimen edges. Crack front location accuracy was enhanced on both fracture toughness specimens by applying a thin coat of flat white spray paint to the specimen edges.

Results

Tension Testing

Failure in all tensile specimens (stitched and unstitched) was preceded by tab delamination. Delamination typically initiated at the tip of the tapered tab end, adjacent to the gage section. When the behavior was first observed, clamping pressure in the test stand hydraulic grips was identified as a probable cause. The initial specimens were gripped with a pressure of 3000 psi, a value that past experience had shown to be appropriate for a specimen of this type. To assess if the grip pressure was playing a role in the observed failure mode, four dummy specimens were cut from the panel trim area and their edges were highlighted with a thin coat of white paint. These coupons were tested in tension at several grip pressures; 2500 psi, 1500 psi, 1000 psi, and 500 psi, 500 psi being the lowest controllable pressure that the test stand's hydraulic grip controller could provide. All of the dummy specimens delaminated at the tab edge without slipping between the grips and tab surfaces. Figure 4 shows one edge of each specimen from the grip pressure experiment. Yellow arrows in the photos indicate the location of the delaminations in each dummy specimen. After completion of the grip pressure trials, the tabs on the first tensile test specimen were removed by inserting a thin blade under the edge of the tab and prying the tab off. The fracture surfaces were examined under a low-power microscope, and a photomicrograph of one tab surface is shown in Figure 5. The tab surface clearly has no traces of adhesive present, except for a small amount along the thin edge of the tab. This indicates that the adhesive did not bond to the tab surface. Based on the two sets of findings, grip pressure was eliminated as a critical factor in the observed failure mode, and the precise cause of the delamination is unknown. However, tab surface contamination and faults with the adhesive are plausible explanations for the bond failure. All other test variables had been consistent with ASTM D3518 recommendations, so the remaining specimens were tested with 3000 psi of grip pressure.

The measured tensile properties are compiled in Table 2. The undesired failure mode calls into question the ultimate tensile strengths reported in this work, and they may differ from those of similar specimens that fail strictly in the gage section. However, there appears to be sufficient data to calculate reliable modulus data for all of the specimens. Specimen #5 in the 72°F / unstitched set had a tensile strength of only 64.4 ksi, only 57% of the strength of the three strongest specimens. If the strength of #5 is taken as an outlier, the remaining five specimens average 103.7 ksi tensile strength with a coefficient of variation (COV) of 9.46%. Similarly to the 72°F data set, the unstitched specimen #5 tested at 180°F exhibited an unexpectedly low strength. Considering it an outlier, the average ultimate strength increases to 107 ksi, and the COV decreases to 6.27%. Alternative values of average, standard deviation, and COV are provided for both sets of unstitched specimens in Table 2. In both specimen sets, modulus and Poisson's ratio averages are comparatively unaffected by the inclusion of specimen #5. Examining the strength averages in Table 2, if we neglect specimen #5 in the unstitched specimen sets, we can conclude that the stitches reduced the tensile strength of the material by 13% and increased the scatter in the strength data.

Post-test photographs of the tensile specimens are provided in Figure 6 - 10. Yellow arrows indicate the location of the ultimate tensile failure for each specimen. The figures clearly show that 22 of 24 tensile specimens failed directly under the tabs. Other damage visible in the specimens is primarily attributable to spring-back of the specimen after final fracture.

Compression

All of the compression specimens exhibited acceptable failure modes, generally near the center of the gage section. The specimen set tested at 72°F displayed brooming failures in four of six specimens. The specimens tested at 180°F all exhibited a buckling failure at an angle to the specimen loading direction. The compression test data are compiled in Table 3. The test specimens are shown in Figure 10 and 12. The increase in test temperature from 72°F to 180°F decreased compressive strength and compressive modulus by 7.5% and 4.2%, respectively, and increased the scatter in those properties.

Inplane Shear

The inplane shear test data are tabulated in Table 4 – 6. Similar to the other specimen types, data from 72°F tests are provided in part (a) of each table. Data from testing at 180°F are provided in part (b). Examination of the data in Table 4 indicates that the specimens tested at 72°F behave consistently, with little scatter. However, the first two specimens tested at 180°F displayed unexpectedly low modulus and strength. Post-test examination of the specimens revealed no indications of anomalies in the specimens, and the data file indicates temperatures close to 180°F. Because no reason could be found for the difference in properties, the shear property data in Table 4(b) are presented two ways, one includes all data from the specimen set, the other assumes that specimens #1 and #2 are outliers.

If we base our assessment of the unstitched material only on the last four specimens, Table 4 indicates that the increase in test temperature from 72°F to 180°F caused a 3% decrease in ultimate shear strength and no decrease in modulus or 5%-offset shear strength. This indicates that the shear properties of the unstitched material are relatively insensitive to temperature over that temperature range. In contrast to that conclusion, Table 5 clearly indicates that the shear properties of the specimens with stitching through the root of the notch were significantly degraded by the elevated test temperature. Shear modulus decreased by 18% with the increase in test temperature. Ultimate and 5%-offset shear strength decreased by 15% and 20%, respectively, at 180°F. Scatter in the data increased at 180°F as well. The specimens with stitching around the root of the notch displayed similar sensitivity to elevated temperature. It is clear from Table 6 that shear modulus decreased by 18% at elevated temperature. Ultimate shear strength was reduced by nearly 19% and the 5%-offset shear strength was reduced by more than 27%. The reason for the high sensitivity of the stitched-around specimens is unclear. However, Table 6(a) shows that shear strength in the room temperature specimens scattered to a larger degree than is seen in either the unstitched or stitched-through specimen sets tested at that temperature.

The previous discussion compared the effects of test temperature on otherwise identical specimen sets. Table 7 compares the effects of both stitching and temperature on shear properties across specimen sets. The knockdowns were calculated for all shear specimen sets relative to unstitched material tested at 72°F. Presented in this manner, it

is clear that stitching has a small effect on room temperature properties, but at elevated temperatures, significant decreases in strength and modulus can be expected.

The unstitched inplane shear specimens displayed subtle indications of surface cracking throughout the region between the specimen notches. This damage was only visible under 10X magnification. Specimens tested at room temperature and at 180°F appeared identical. Damage within the specimens with stitching through the root of the notch appeared to be concentrated along the stitch line. Close examination of these specimens reveals a small wrinkle through the gage section directly over the central stitch line. This wrinkle may be attributable to microbuckling of 90° fiber bundles between resin rich regions around the stitches and shear deformation within those regions. The specimens tested at 180°F have a more prominent wrinkle. Similar to the other specimens, this wrinkle is only visible under the smooth covering of strain gage adhesive. Damage in the specimens with stitch lines spanning the notch region was mostly seen between the two lines of stitches. The most prominent sign of damage in specimens tested at 72°F and 180°F was small striations oriented between notches. These can only be seen in regions covered with a thin, smooth layer of strain gage mounting adhesive. Examination of the edges in the notch region reveals no signs of delamination in any of the shear specimens. The lack of scoring in the grip sections of the specimens show that all specimens were held immobile in the grips and that load was applied in the manner expected during testing, which lends confidence to the shear strength data generated in this work. Post-test photographs of shear specimens were not included in this report because the macroscopic signs of damage were too subtle to be captured via that method.

Mode I Fracture Toughness

The load, displacement, and crack length data from the DCB tests were analyzed by the Modified Compliance Calibration method of the test standard. The resultant R-curves for DCB specimens are compiled in Table 8. The critical fracture toughness for each specimen is listed in Table 9. To avoid variability due to geometric variation in the Teflon insert, G_{IC} is taken as the apparent fracture toughness at a point at which the crack front propagated 5 mm. from the insert edge. Note that these data are for specimens without through-thickness stitching. Testing of stitched DCB specimens proved to be impracticable.

Testing of the first stitched DCB specimen revealed uncertainties related to the test specimen and analysis method. Because of the difference in stitch angles relative to the laminate midplane, the vertical stitches carried more of the crack opening load than the angled stitches. As a result, as the crack began to extend from the Teflon insert, the arms of the specimen exhibited noticeable twisting and the crack front became highly skewed. The crack propagated several stitches before stopping. Increasing loads eventually caused the stitches to fracture, and the crack to propagate the full length of the specimen. The non-uniformity of the applied load and the highly skewed crack front during crack extension were inconsistent with the assumptions of the test specification. However, the observed behavior is consistent with analytical predictions of stitched composite behavior^{6,7}. Further DCB testing was deferred until in-depth examination of the test results for the first specimen can evaluate the validity of the test results. In the end, time constraints prevented completion of stitched DCB specimen testing, so those results will not be included in this report.

Mode II Fracture Toughness

The results of Mode II fracture toughness testing are tabulated in Table 10. Fracture toughness values are provided for the first loading (non-precracked) and the second loading (precracked). During compliance calibration loadings of the stitched specimens, some variation in the applied load was caused by the unevenness of the stitched IML surface. Fitting least-square linear curves to the stitched specimen data was therefore less accurate than with the specimens without stitching. These uncertainties result in more scatter in apparent fracture toughness than the unstitched specimens. Even with the additional scatter, the data indicate that the stitches provided an increase in Mode II fracture toughness.

Concluding Remarks

Several material properties (modulus, strengths, and fracture toughness) of a textile composite have been characterized to provide input data to analytical models of PRSEUS structure. Tensile, compressive, shear, and fracture toughness properties have been measured at ambient and elevated temperatures, and with and without

through-thickness stitching. Tensile specimens exhibited tab-related failure modes, which may have resulted in overly conservative estimates for tensile strength. A test temperature of 180°F had little effect on tensile properties in comparison to similar specimens tested at ambient temperature. Stitching reduced tensile strength by approximately 13%. Compressive properties were reduced by the elevated test temperature by 4% – 8%. Elevated test temperature had no significant impact on shear properties of unstitched material. Similarly, the presence of stitching alone had only small effects (less than 6% reductions) on shear properties at ambient temperature. However, the presence of stitching at elevated test temperatures resulted in reductions in shear modulus of up to 17% and reductions in shear strength of up to 23% relative to unstitched, room temperature strength. The effect of stitching could not be assessed on Mode I fracture toughness because of unsteady crack growth. Mode II fracture toughness was measured on both stitched and unstitched specimen, and the stitching clearly increased G_{IIC} but caused an increase in the variability of that property.

References

1. Velicki, Alex and D. Jegley. PRSEUS Development For The Hybrid Wing Body Aircraft, 11th AIAA Aviation Technology, Integration, and Operations (ATIO) Conference; AIAA-2011-7025.
2. Jegley, Dawn C, and A. Velicki. Status of Advanced Stitched Unitized Composite Aircraft Structure, 51st AIAA Aerospace Sciences Meeting; AIAA-2013-0410.
3. Dow, Marvin. and H B. Dexter. Development of Stitched, Braided, and Woven Composite Structures In the Act Program and at Langley Research Center (1985 to 1997) – Summary and Bibliography. NASA TP-97-206234, November 1997, <http://ntrs.nasa.gov/?N=123&Ntk=All&Ntt=Dow%2C%20marvin&Ntx=mode+matchallpartial>
4. Dexter, H. Benson. and B. A. Stein. Advanced Composite Materials for Airframe Structures, Fiber-TEX 1987- First Conference on Advanced Engineering Fibers and Textile Structures for Composites, NASA CP 3001.
5. Jegley, Dawn C. Behavior of Frame-Stiffened Composites Panels With Damage. 54th AIAA/ASME/ASCE/AHS/ASC Structures, Structural Dynamics, and Materials Conference; AIAA 2013-1738.
6. Glaessgen, E.H. and I. S. Raju, Debonding of Stitched Composite Sandwich Structures, 41st Structures, Structural Dynamics, and Materials Conference and Exhibit; AIAA-2000-1614.
7. Glaessgen, E.H., I. S. Raju, and C. C. Poe. Fracture Mechanics Analysis of Stitched Stiffener-Skin Debonding, 39th AIAA/ASME/ASCE/AHS/ASC Structures, Structural Dynamics, and Materials Conference and Exhibit; AIAA-98-2022.

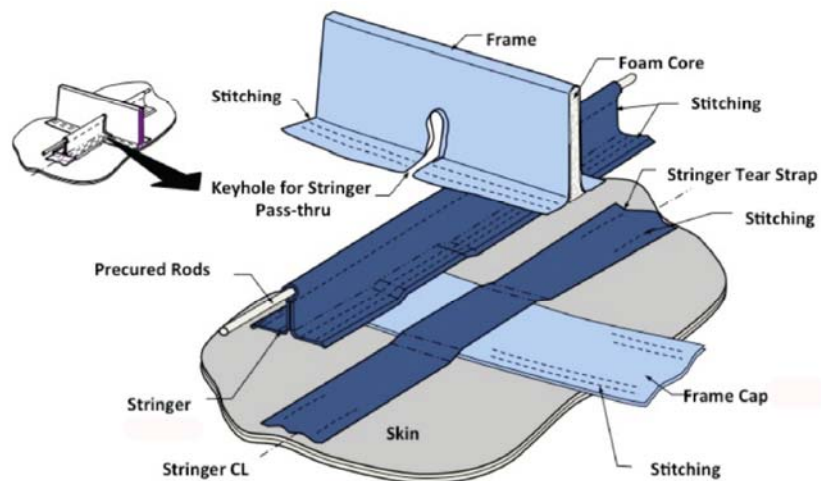


Figure 1. PRSEUS structure stringer-frame intersection

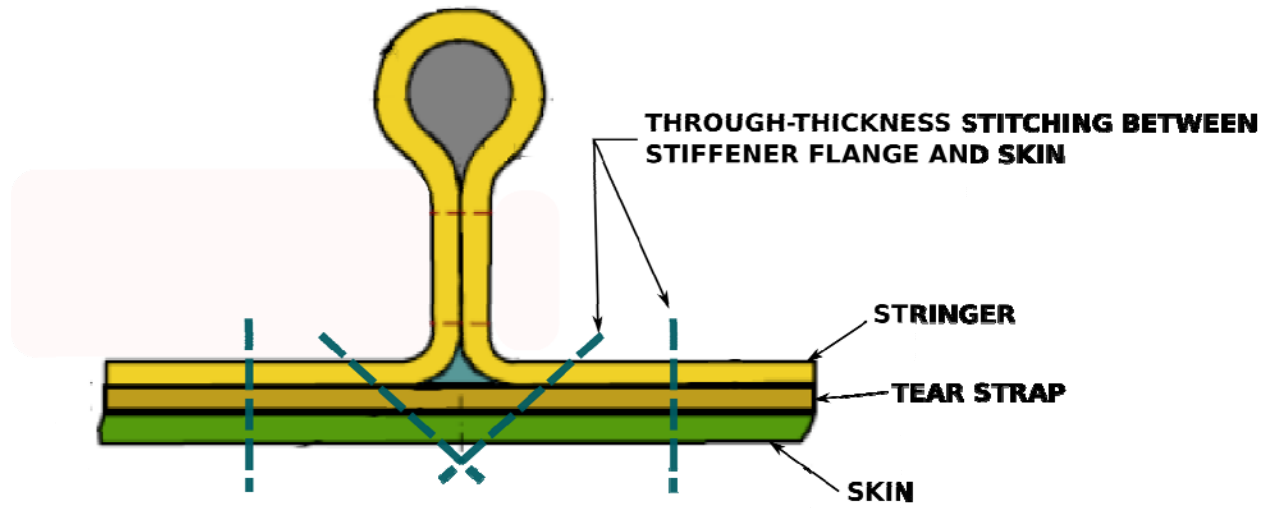


Figure 2. Cross-section of typical PRSEUS skin, tear strap and stringer

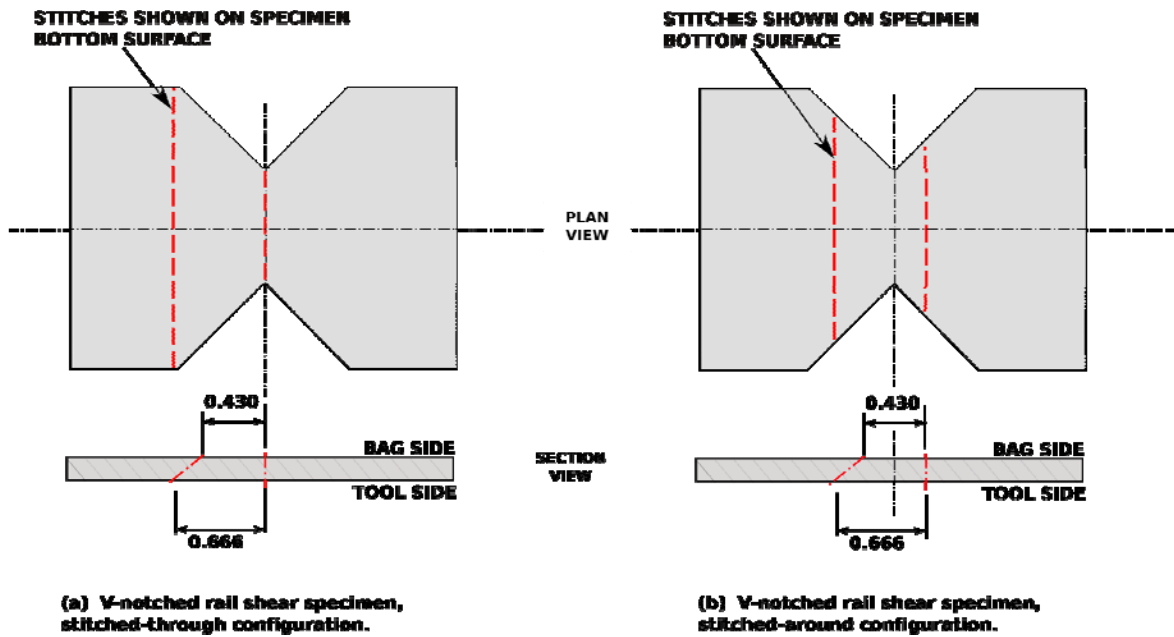


Figure 3. Stitching scheme used in V-notched shear specimen preparation

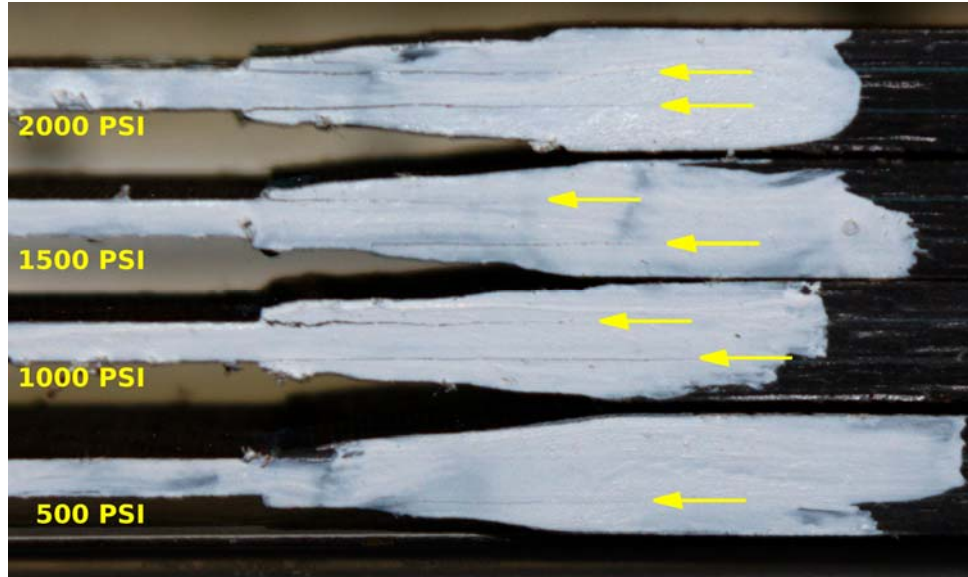


Figure 4. Specimens used in the grip pressure experiment, showing typical disbond failure as seen in all tensile test specimens. Arrows indicate tab delaminations. Similar tab failures were observed in all tensile specimens.

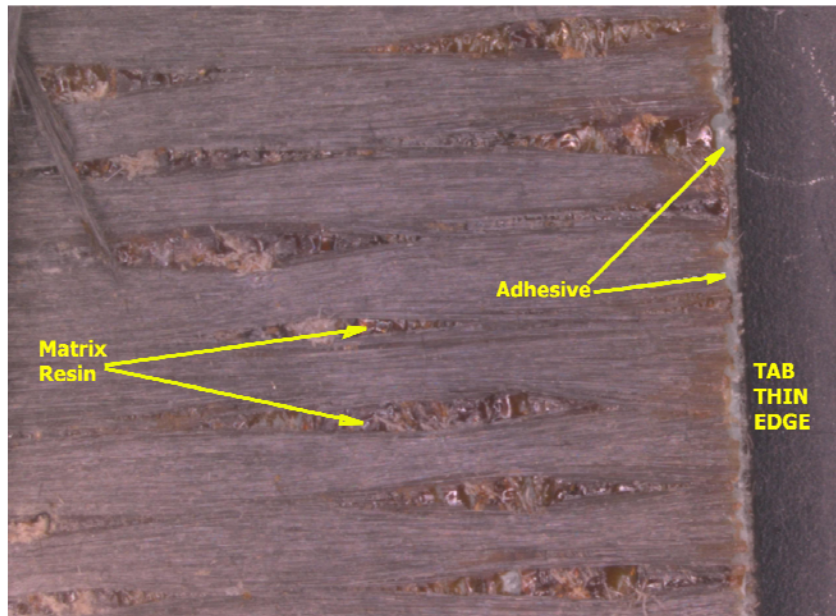


Figure 5. Tensile specimen tab fracture surface after delamination

Table 2. Tensile test results

(a) 72°F

Specimen	Unstitched			Stitched		
	Strength, ksi	Modulus, Msi	Poisson's Ratio	Strength, ksi	Modulus, Msi	Poisson's Ratio
1	90.2	8.36	0.057	91.9	8.34	0.057
2	96.4	8.23	0.052	89.3	8.05	0.052
3	109.9	8.58	0.060	92.6	7.92	0.060
4	111.8	8.41	0.057	91.1	7.95	0.057
5	62.4	8.16	0.051	87.4	8.17	0.051
6	110.4	8.67	0.053	80.9	7.90	0.053
Average	96.8 [103.7] ^b	8.40	0.055	88.9	8.05	0.055
Standard Deviation	19.0 [9.81] ^b	0.20	0.003	4.33	0.17	0.003
COV ^a	19.6% [9.46%] ^b	2.36%	6.19%	4.87%	2.12%	6.19%

(b) 180°F

Specimen	Unstitched			Stitched		
	Strength, ksi	Modulus, Msi	Poisson's Ratio	Strength, ksi	Modulus, Msi	Poisson's Ratio
1	100.0	8.41	0.056	97.4	8.18	0.056
2	112.8	8.34	0.046	90.7	8.06	0.040
3	111.0	8.44	0.043	84.4	8.56	0.057
4	100.1	8.31	0.050	97.7	8.01	0.062
5	57.7	8.20	0.050	96.3	7.69	0.041
6	113.0	7.95	0.047	94.0	7.93	0.050
Average	99.1 [107.4] ^b	8.27	0.049	93.4	8.07	0.051
Standard Deviation	21.2 [6.74] ^b	0.18	0.005	5.14	0.29	0.009
COV ^a	21.4% [6.27%] ^b	2.19%	9.35%	5.50%	3.58%	18.1%

Note: Tab delamination on all tensile specimens may have induced premature tensile failure. The reported tensile data may underestimate actual material strength and modulus.

^a Coefficient of variation

^b Considering specimen #5 of both unstitched specimen sets an outlier

Table 3. Compression test results, stitched material

Specimen	72°F		180°F	
	Strength, ksi	Modulus, Msi	Strength, ksi	Modulus, Msi
1	90.2	--	91.5	7.52
2	90.7	--	78.5	7.51
3	88.5	--	81.6	6.65
4	85.7	7.65	82.7	7.30
5	78.6	7.46	71.3	7.30
6	93.1	7.56	81.4	7.17
Average	87.8	7.56	81.2	7.24
Standard Deviation	5.14	0.09	6.54	0.32
COV^a	5.85%	1.19%	8.05%	4.42%

-- No strain data recorded

^a Coefficient of variation

Table 4. Inplane shear test results, unstitched material

(a) 72°F

Specimen	Chord Modulus, Msi	Ultimate Strength, ksi	5% Offset Strength, ksi
1	0.73	13.0	-- ^a
2	0.75	14.2	13.1
3	0.73	14.4	13.1
4	0.67	14.6	13.1
5	0.73	14.5	13.0
6	0.72	14.6	12.9
Average	0.72	14.4	13.1
Standard Deviation	0.03	0.17	0.04
COV^b	3.67%	1.15%	0.33%

(b) 180°F

Specimen	Chord Modulus, Msi	Ultimate Strength, ksi	5% Offset Strength, ksi
1	0.54	11.2	9.05
2	0.60	11.2	10.1
3	0.74	14.3	13.2
4	0.71	14.1	13.4
5	0.75	13.4	12.9
6	0.72	14.1	13.0
Average	0.68 [0.73]^c	13.1 [13.99]^c	11.9 [13.11]^c
Standard Deviation	0.09 [0.02]^c	1.34 [0.368]^c	1.70 [0.211]^c
COV^b	13.1% [2.59%]^c	10.2% [2.63%]^c	14.3% [1.61%]^c

a Strain gage failure prior to this point

b Coefficient of variation

c With specimens #1 and #2 considered to be outliers

Table 5. Inplane shear test results, stitched through the notch

(a) 72°F

Specimen	Chord Modulus, Msi	Ultimate Strength, ksi	5% Offset Strength, ksi
1	0.76	14.4	13.0
2	-- ^a	-- ^a	-- ^a
3	0.73	14.0	12.9
4	0.73	13.7	12.9
5	0.74	13.2	12.7
6	0.70	13.8	12.7
Average	0.73	13.7	12.8
Standard Deviation	0.01	0.27	0.13
COV^b	1.87%	2.00%	0.99%

(b) 180°F

Specimen	Chord Modulus, Msi	Ultimate Strength, ksi	5% Offset Strength, ksi
1	0.61	11.8	10.3
2	0.59	11.5	10.3
3	0.61	11.5	10.1
4	0.60	11.9	10.4
5	0.61	12.1	10.5
6	0.57	10.9	9.5
Average	0.59	11.6	10.3
Standard Deviation	0.02	0.40	0.19
COV^b	2.71%	3.44%	10.3%

^a Data acquisition failure

^b Coefficient of variation

Table 6. Inplane shear test results, stitched around notch

(a) 72°F

Specimen	Chord Modulus, Msi	Ultimate Strength, ksi	5% Offset Strength, ksi
1	0.76	14.6	14.6
2	0.76	15.9	12.8
3	0.75	14.4	12.8
4	0.76	13.6	12.9
5	0.76	15.5	14.8
6	0.78	14.9	13.2
Average	0.76	14.9	13.8
Standard Deviation	0.01	0.80	1.00
COV^a	1.37%	5.38%	7.22%

(b) 180F

Specimen	Chord Modulus, Msi	Ultimate Strength, ksi	5% Offset Strength, ksi
1	0.63	11.8	10.1
2	0.61	11.5	10.0
3	0.62	11.6	9.9
4	0.64	12.1	10.2
5	0.63	13.0	10.1
6	0.63	12.0	10.1
Average	0.63	12.0	10.0
Standard Deviation	0.01	0.53	0.10
COV^a	1.17%	4.43%	1.00%

^a Coefficient of variation

Table 7. Knockdown on shear properties due to stitching and elevated test temperature. All knockdowns are relative to unstitched material tested at 72°F, and considering specimens #1 and #2 in Table 4(b) to be outliers.

Property	Test Temperature	Stitching		
		US	SA	ST
Shear Modulus	72°F	--	5.9%	0.8%
	180°F	1.3%	-13.2%	-17.4%
Ultimate Shear Strength	72°F	--	2.8%	-5.5%
	180°F	-3.2%	-16.6%	-23.2%
5% Offset Shear Strength	72°F	--	-5.5%	-2.2%
	180°F	0.3%	-23.2%	-21.1%

US = unstitched; SA = stitched around notch; ST = stitched through notch

Table 8. Mode I fracture toughness testing as a function of crack length at ambient temperature

Specimen #1		Specimen #2		Specimen #3		Specimen #4		Specimen #5		Specimen #6	
Crack Length, in	G_I , in·lbf/in ²										
1.59	0.17	1.84	2.61	1.81	2.14	1.86	2.60	1.79	2.06	1.81	2.07
1.68	0.42	1.86	2.69	1.83	2.36	1.88	2.92	1.86	2.28	1.84	2.17
1.71	2.39	1.91	2.89	1.86	2.44	1.94	3.06	2.05	2.90	1.92	2.23
1.75	2.56	2.08	3.42	2.11	3.05	1.99	3.09	2.25	3.35	1.93	2.24
1.79	2.67	2.31	3.93	2.24	3.52	2.16	3.41	2.40	3.36	2.09	2.46
1.97	3.22	2.49	3.86	2.46	3.93	2.37	3.51	2.56	3.17	2.31	2.76
2.13	3.40	2.67	3.73	2.72	3.65	2.52	3.17	2.73	2.98	2.48	2.85
2.31	3.28	2.85	3.78	2.88	3.72	2.72	2.99	2.94	3.12	2.66	2.88
2.58	3.28	3.06	3.78	3.07	3.38	2.93	3.05	3.01	3.21	2.81	2.98
2.78	3.09	3.28	3.53	3.26	3.36	3.25	3.35	3.22	3.32	3.02	3.14
2.98	3.27	3.46	3.26	3.47	3.41	3.30	3.01	3.34	3.13	3.24	3.06
3.19	3.34	3.50	3.21	3.64	3.52	3.45	3.14	3.65	3.16	3.43	2.89
3.37	3.50	3.68	3.01	3.70	3.34	3.68	3.03	3.65	2.76	3.71	3.05
3.55	3.34	3.69	2.99	3.78	3.25	3.71	2.77	3.70	2.81	3.74	2.67
3.60	2.98	3.72	3.04	3.81	3.30	3.73	2.82	3.74	2.79	3.81	2.67
3.63	2.86	3.80	3.23	3.83	3.29	3.78	2.64	3.81	2.80	3.82	2.58
3.65	2.75	3.84	3.23			3.81	2.67	3.86	2.83	3.84	2.57
3.67	2.75					3.86	2.77			3.84	2.59
3.76	2.79					3.84	2.72				

Table 9. Precracked G_{IC} , unstitched material tested at 72°F.

Specimen	G_{IC} , lbf-in/in ²
1	2.24
2	2.36
3	1.98
4	2.28
5	2.26
6	2.29
Average	2.23
Standard Deviation	0.13
COV[†]	5.83%

[†] Coefficient of variation

Table 10. Mode II fracture toughness of PRSEUS laminates, tested at 72°F and 180°F, with and without through-thickness stitching.

	Test Temperature, °F	Specimen	Specimen G_{II} , in-lbf/in ²		Average G_{II} (SD / COV) [†] , in-lbf/in ²	
			Non-Precracked	Precracked	Non-Precracked	Precracked
Unstitched	72	1	1.96	1.53	2.11 (0.37 / 17.5%)	1.63 (0.110 / 6.75%)
		2	2.30	1.69		
		3	2.22	1.46		
		4	1.99	1.74		
		5	1.55	1.69		
		6	2.66	1.69		
	180	1	2.01	1.57	2.03 (0.100 / 4.93%)	1.69 (0.130 / 7.69%)
		2	2.07	--		
		3	2.06	1.87		
		4	1.97	1.59		
		5	2.18	1.77		
		6	1.89	1.62		
Stitched	72	1	3.06	3.85	2.49 (0.550 / 22.1%)	3.02 (0.710 / 23.5%)
		2	2.61	2.51		
		3	2.37	2.05		
		4	1.63	3.46		
		5	3.07	2.66		
		6	2.24	3.58		
	180	1	2.85	2.91	2.97 (0.419 / 14.1%)	3.66 (0.739 / 20.2%)
		2	2.91	2.80		
		3	--	--		
		4	3.19	4.30		
		5	3.51	4.29		
		6	2.38	3.98		

[†] (Standard deviation / Coefficient of variation)

-- Missing or faulty data

Appendix: Post-test photographs of test specimens

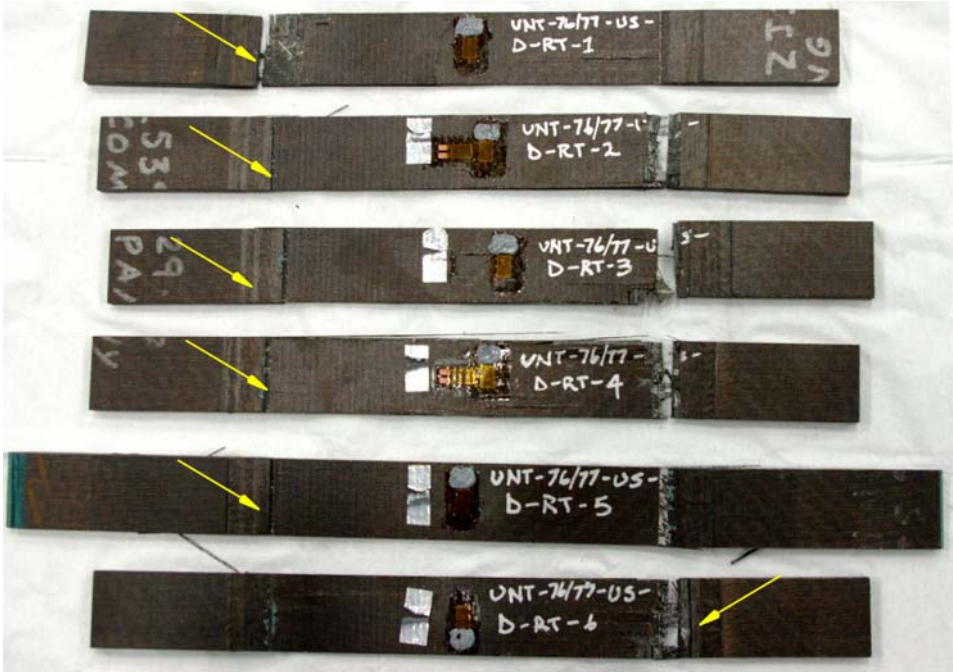


Figure 6. Tensile specimens with final failure location marked, no stitching, tested at 72°F.

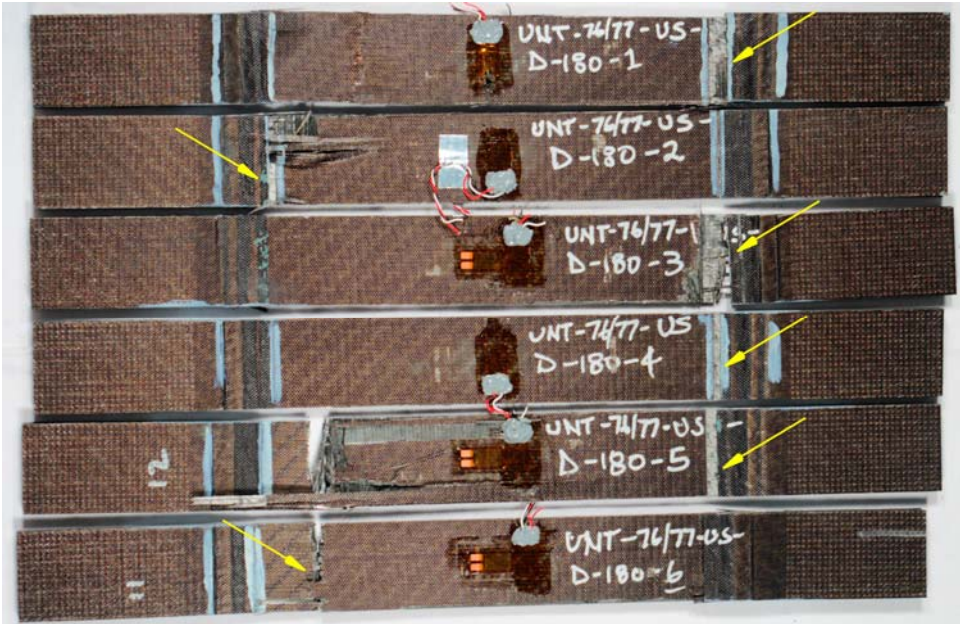


Figure 7. Tensile specimens with final failure location marked, no stitching, tested at 180°F.



Figure 8. Tensile specimens with final failure location marked, stitched material, tested at 72°F.



Figure 9. Tensile specimens with final failure location marked, stitched material, tested at 180°F.

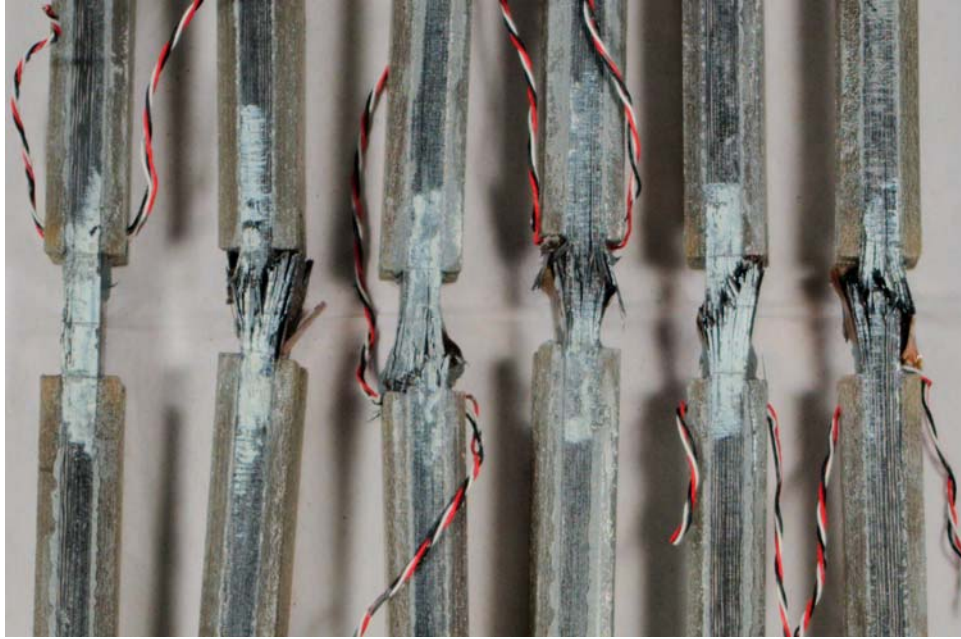


Figure 10. Edge-on view of unnotched compression specimens tested at 72°F



Figure 11. Edge-on view of unnotched compression specimens tested at 180°F

REPORT DOCUMENTATION PAGE

*Form Approved
OMB No. 0704-0188*

The public reporting burden for this collection of information is estimated to average 1 hour per response, including the time for reviewing instructions, searching existing data sources, gathering and maintaining the data needed, and completing and reviewing the collection of information. Send comments regarding this burden estimate or any other aspect of this collection of information, including suggestions for reducing this burden, to Department of Defense, Washington Headquarters Services, Directorate for Information Operations and Reports (0704-0188), 1215 Jefferson Davis Highway, Suite 1204, Arlington, VA 22202-4302. Respondents should be aware that notwithstanding any other provision of law, no person shall be subject to any penalty for failing to comply with a collection of information if it does not display a currently valid OMB control number.
PLEASE DO NOT RETURN YOUR FORM TO THE ABOVE ADDRESS.

1. REPORT DATE (DD-MM-YYYY) 01-10-2013		2. REPORT TYPE Technical Memorandum		3. DATES COVERED (From - To)	
4. TITLE AND SUBTITLE Material Property Characterization of AS4/VRM-34 Textile Laminates				5a. CONTRACT NUMBER	
				5b. GRANT NUMBER	
				5c. PROGRAM ELEMENT NUMBER	
				5d. PROJECT NUMBER	
6. AUTHOR(S) Grenoble, Ray W.; Johnston, William M.				5e. TASK NUMBER	
				5f. WORK UNIT NUMBER 699959.02.22.07.01.01	
				8. PERFORMING ORGANIZATION REPORT NUMBER L-20276	
7. PERFORMING ORGANIZATION NAME(S) AND ADDRESS(ES) NASA Langley Research Center Hampton, VA 23681-2199				10. SPONSOR/MONITOR'S ACRONYM(S) NASA	
9. SPONSORING/MONITORING AGENCY NAME(S) AND ADDRESS(ES) National Aeronautics and Space Administration Washington, DC 20546-0001				11. SPONSOR/MONITOR'S REPORT NUMBER(S) NASA/TM-2013-218050	
12. DISTRIBUTION/AVAILABILITY STATEMENT Unclassified - Unlimited Subject Category 01 Availability: NASA CASI (443) 757-5802					
13. SUPPLEMENTARY NOTES					
14. ABSTRACT Several material properties (modulus, strengths, and fracture toughness) of a textile composite have been evaluated to provide input data to analytical models of PRSEUS structure. The material system is based on warp-knitted preforms of AS4 carbon fibers and VRM-34 epoxy resin, which have been processed via resin infusion and oven curing. Tensile, compressive, shear, and fracture toughness properties have been measured at ambient and elevated temperatures. All specimens were tested in as-fabricated (dry) condition. Specimens were tested with and without through-thickness stitching.					
15. SUBJECT TERMS Composites; Hybrid wing body; PRSEUS; Stitching; Textiles					
16. SECURITY CLASSIFICATION OF:			17. LIMITATION OF ABSTRACT	18. NUMBER OF PAGES	19a. NAME OF RESPONSIBLE PERSON
a. REPORT	b. ABSTRACT	c. THIS PAGE			STI Help Desk (email: help@sti.nasa.gov)
U	U	U	UU	23	19b. TELEPHONE NUMBER (Include area code) (443) 757-5802